The Astrophysical Journal, 887:127 (10pp), 2019 December 20 https://doi.org/10.3847/1538-4357/ab505d

On the Origin of SN 2016hil—A Type II Supernova in the Remote Outskirts of an Elliptical Host

Ido Irani[1], Steve Schulze[1], Avishay Gal-Yam[1], Ragnhild Lunnan[2], Thomas G. Brink[3], WeiKang Zheng[3], Alexei V. Filippenko[3,4,9], Yi Yang[2], Thomas de Jaeger[3], Peter E. Nugent[3,5], Mansi M. Kasliwal[6], Christoffer Fremling[6], James Don Neill[6], Umaa Rebbapragada[7], Frank J. Masci[8], Jesper Sollerman[2], and Ofer Yaron[1]
[1] Department of Particle Physics and Astrophysics, Weizmann Institute of Science, 234 Herzl St., 76100 Rehovot, Israel
[2] The Oskar Klein Centre & Department of Astronomy, Stockholm University, AlbaNova, SE-106 91 Stockholm, Sweden
[3] Department of Astronomy, University of California, Berkeley, CA 94720-3411, USA
[4] Miller Institute for Basic Research in Science, University of California, Berkeley, CA 94720, USA
[5] Lawrence Berkeley National Laboratory, Berkeley, California 94720, USA
[6] Division of Physics, Math, and Astronomy, California Institute of Technology, Pasadena, CA 91125, USA
[7] Jet Propulsion Laboratory, California Institute of Technology, Pasadena, CA 91109, USA
[8] IPAC, California Institute of Technology, 1200 E. California Boulevard, Pasadena, CA 91125, USA
Received 2019 April 11; revised 2019 September 26; accepted 2019 October 21; published 2019 December 16

Abstract

Type II supernovae (SNe) stem from the core collapse of massive ($>8\,M_{\odot}$) stars. Due to their short lifespan, we expect a very low rate of such events in elliptical hosts, where the star formation rate is low, and which are mostly comprised of an old stellar population. SN 2016hil (iPTF16hil) is an SN II located in the extreme outskirts of an elliptical galaxy at $z = 0.0608$ (projected distance 27.2 kpc). It was detected near peak ($M_r \sim -17$ mag) 9 days after the last non-detection. The event has some potentially peculiar properties: it presented an apparently double-peaked light curve, and its spectra suggest low metallicity content ($Z < 0.4\,Z_{\odot}$). We place a tentative upper limit on the mass of a potential faint host at $\log \frac{M}{M_{\odot}} = 7.27^{+0.43}_{-0.24}$ using deep optical imaging from Keck/LRIS. In light of this, we discuss the possibility of the progenitor forming locally and other more exotic formation scenarios such as a merger or common-envelope evolution causing a time-delayed explosion. Further observations of the explosion site in the UV are needed in order to distinguish between the cases. Regardless of the origin of the transient, observing a population of such seemingly hostless SNe II could have many uses, including an estimate the amount of faint galaxies in a given volume, and tests of the prediction of a time-delayed population of core-collapse SNe in locations otherwise unfavorable for the detection of such events.

Unified Astronomy Thesaurus concepts: Core-collapse supernovae (304); Elliptical galaxies (456); Dwarf galaxies (416); Early-type galaxies (429); Binary stars (154)

1. Introduction

The progenitors of Type II supernovae (SNe) are recognized to be massive stars ($>8\,M_{\odot}$; e.g., Smartt 2009) at the ends of their lives. Owing to their short lifespan, we expect a very low rate of such events far from star-forming regions (James & Anderson 2006), and in particular in early-type galaxies, which mostly consist of an old stellar population (i.e., of low-mass stars). Indeed, a systematic analysis of the hosts of SNe (Hakobyan et al. 2012) reveals no core-collapse SNe (CCSNe) in elliptical (E) hosts, and only two cases in lenticular (S0) hosts, in comparison to 147 SNe Ia in such galaxies from the same sample. The few hosts of SNe II/Ib previously thought to be early-type galaxies were misclassified according to this analysis. Another analysis of these debated cases (Suh et al. 2011) demonstrates a systematically bluer color and stronger radio emission of the supposed early-type hosts of CCSNe compared to early-type hosts of SNe Ia—signatures of recent star formation (SF). More generally, a fraction of early-type galaxies have demonstrated some SF (see, e.g., Crocker et al. 2011; Kaviraj et al. 2007, or Kaviraj et al. 2008). It has been suggested that minor mergers are the main mechanism of such residual star formation (Kaviraj et al. 2009). This gives reasons to expect a residual rate of CCSNe in early-type galaxies. Such is the case of the SN II A399 11 19 0 (Graham et al. 2012), which appeared in a galaxy with elliptical morphology demonstrating evidence of weak recent SF through Hα emission.

There are also possible reasons to expect a residual population of CCSNe in regions with no recent SF. Zapartas et al. (2017) suggest that a significant fraction (~15%) of CCSNe are caused by mass transfer between a pair of intermediate-mass (4–8 $M_{\odot}$) binaries, occurring up to 200 Myr after stellar birth ("late" events). Similarly, Soker (2019) outlines several possible mechanisms through which common-envelope evolution may terminate in CCSNe. Such scenarios would involve a secondary star or stripped core spiraling into the envelope of a larger primary star, resulting in an SN explosion.

From an observational point of view, there have been rare cases of non-Ia SNe in early-type hosts, where no nearby SF could be measured. For example, the SN Ibn PS1-12sk (Sanders et al. 2013) occurred in the local environment of an E host (projected separation 28.1 kpc). Hosseinzadeh et al. (2019) analyze deep ultraviolet (UV) images of the event obtained with the *Hubble Space Telescope (HST)*, and find no measurable SF activity in the region. In light of this, it has been suggested that the progenitor of PS1-12sk might not have been a massive star, and some alternatives have been suggested. Similarly, "Ca-rich" SNe Ib (Filippenko et al. 2003) are thought to be the product of interactions between two white

[9] Miller Senior Fellow.

dwarfs and not a result of core collapse (Perets et al. 2010; Waldman et al. 2011), as they essentially always occur in or near old stellar environments (Lunnan et al. 2017). For example, the environment of SN 2005cz (Kawabata et al. 2010) was investigated thoroughly and demonstrated to exhibit no SF (Perets et al. 2011).

Finally, early-type galaxies may have dwarf satellites that present some SF activity. Given the limiting magnitudes (∼22.5 mag) of the Sloan Digital Sky Survey (SDSS; York et al. 2000) and the Panoramic Survey Telescope and Rapid Response System 1 (PS1; Chambers et al. 2016), we would be unable to detect galaxies fainter than $M \approx -14.5$ mag at a redshift $z = 0.06$, which is relevant for this study. We certainly expect a non-negligible fraction of CCSNe to occur in such hosts (Arcavi et al. 2010).

In the past decade, automated and systematic surveys have increased the rate of SN discoveries by orders of magnitude. These include the Palomar Transient Factory (PTF; Law et al. 2009), its inheritor the intermediate Palomar Transient Factory (iPTF; Kulkarni 2013), the All Sky Automated Survey for Supernovae (ASAS-SN; Shappee et al. 2014), the Asteroid Terrestrial-impact Last Alert System (ATLAS; Tonry et al. 2018), PS1, and the *Gaia* Photometric Science Alerts (Wyrzykowski et al. 2012). For example, (i)PTF discovered more than 4000 SNe, of which ∼950 were core-collapse events. This provides access to populations that occur at a rate of ∼1% of all core-collapse events. Within the next year, the Zwicky Transient Facility (ZTF; Bellm et al. 2019) is expected to observe a similar number of events. This will open a window for studying new and exotic populations of transients, of which few events were observed in the past or that are completely unknown.

Here we present the case of SN 2016hil. The event was discovered (Kasliwal & Cao 2018) and classified (Irani 2019) by iPTF as a spectroscopically regular SN II (e.g., Filippenko 1997; Gal-Yam 2017). SN 2016hil occurred in an unusual location—the outskirts of an elliptical galaxy. We describe our spectroscopic and photometric observations in Section 2, present our findings concerning the transient and its host galaxy in Section 3, and discuss possible origins for the event in Section 4. Throughout this paper we assume $H_0 = 67.11\,\mathrm{km\,s^{-1}\,Mpc^{-1}}$ and a ΛCDM cosmology with $\Omega_m = 0.32$ and $\Omega_\Lambda = 0.68$ (Planck Collaboration et al. 2014).

2. Observations

2.1. Discovery, Classification, and Host Galaxy

SN 2016hil was detected using the 48 inch telescope at Palomar Observatory (P48), on 2016 October 22 (UT dates are used throughout this paper) at 07:55 (JD 2457683.801), in the *r* band (20.29 ± 0.12 mag) and was observed in the *g* band (20.34 ± 0.13 mag) 40 minutes later. The source was at $\alpha = 01^{\rm h}10^{\rm m}24\overset{\rm s}{.}75$, $\delta = +14°12'15\overset{''}{.}5$ (J2000). The last non-detection was 9 days before the explosion down to a 3σ limit of 20.89 mag in the *r* band, although an earlier marginal 3σ detection in the *r* band was later identified (see Section 2.3).

In Figure 1, we present the unusual location of the event: on the outskirts of the elliptical galaxy SDSS J011024.51 +141238.7. This galaxy is observed at a redshift $z = 0.06079$, consistent with the redshift derived from the Hα emission line in the spectra of SN 2016hil (see Section 2.2).

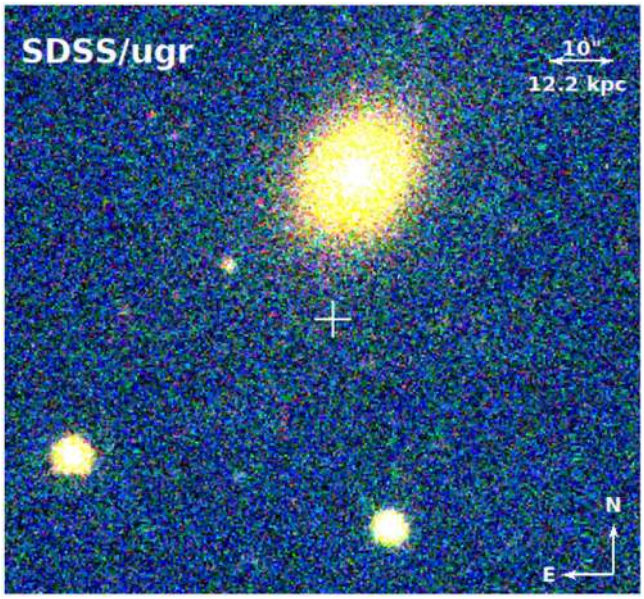

Figure 1. Host galaxy of SN 2016hil as observed by SDSS in late 2004 in the *ugr* bands. The event location is marked with a white cross. SN 2016hil was observed $23\overset{''}{.}1 \pm 0\overset{''}{.}3$ from the region of maximal brightness in the host, corresponding to a projected separation of 27.2 ± 0.4 kpc, assuming a host redshift of $z = 0.06079$.

Table 1
Log of Optical Spectra of SN 2016hil

Date	Δt (day)[a]	Instrument	Exp. Time (s)	Airmass
2016 Oct 26	4	P200/DBSP	600 × 2	1.10
2016 Oct 31	9	Keck/LRIS	1850	1.35
2016 Nov 02	11	Keck/LRIS	1160	1.07
2016 Nov 28	37	Keck/LRIS	870	1.41

Note.
[a] Relative to first detection.

2.2. Optical Spectroscopy

We collected four optical spectra during a period of 40 days when SN 2016hil was visible. On 2016 October 26, the first spectrum of the SN was obtained using the Double Beam Spectrograph (DBSP; Oke & Gunn 1982) mounted on the Palomar 200 inch Hale telescope (P200). The gratings of 600/4000 and 316/7500 were used for the blue and red cameras, respectively, with the D55 dichroic. The data were reduced using standard procedures, including bias and flatfield corrections, one-dimensional spectral extraction, wavelength calibration with comparison lamps, and flux calibration using observations of standard stars observed during the same night and at approximately similar airmasses to the SN.

Three additional spectra were obtained with the Low Resolution Imaging Spectrometer (LRIS; Oke et al. 1995) on the 10 m Keck I telescope. The gratings of 300/3400 and 300/8500 were used for the blue and red cameras, respectively, with the 560 dichroic. The data were reduced using the `LRIS automated reduction pipeline` (`LPipe`) (Perley 2019), and are made available to the public on WISeREP (Yaron & Gal-Yam 2012). In Table 1 we report our spectral observation log and in Figure 2 we present the full set of spectra. They exhibit broad hydrogen emission features that

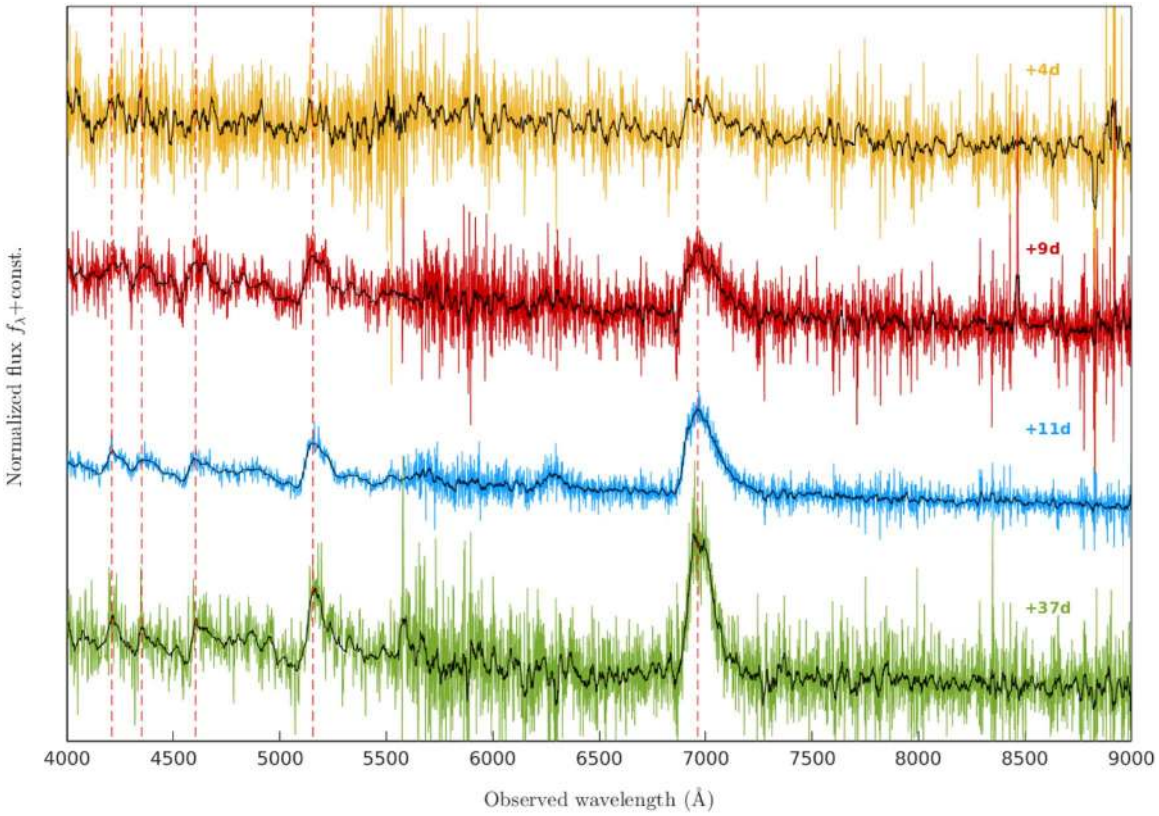

Figure 2. Spectral evolution of SN 2016hil. The spectra (color) are overlaid with a smooth version (black), and labeled according to their observation time relative to first detection. The red dashed lines correspond to redshifted hydrogen lines Hα through Hε (from right to left). Spectra are trimmed below 4000 Å owing to the low signal-to-noise ratio (S/N) at these wavelengths.

evolve rapidly throughout the observation period, based on which SN 2016hil is classified as an SN II.

2.3. Optical Photometry

After the detection, follow-up observations were made using the Spectral Energy Distribution Machine (SEDM; Blagorodnova et al. 2018) mounted at the 60 inch telescope at Palomar Observatory (P60), in addition to routine monitoring with the P48. Photometry was acquired with the SDSS *g* and Mould-*R* bands for the P48 images, and with the SDSS *gri* bands for the P60 images. Mould-*R* was then converted to the SDSS *r* band using the Lupton color equations (2005).[10] Since SN 2016hil is located on a simple background, we chose to use aperture photometry in order to extract source fluxes. This was done by designing custom apertures and annuli with the MATLAB Astronomy & Astrophysics Toolbox[11] (Ofek 2014). We calibrated zero-points with SDSS stars. Using the images from the days previous to first detection, we summed the non-detection fluxes and derived summed non-detection limits to constrain the shape of the light curve before peak brightness (not including the flux from the marginal 3σ detection at $t = -10$ days). We repeated this procedures for the epochs after rebrightening observed at $t \approx 32$ days, when poor weather conditions at Palomar prevented further photometric observations.

Moreover, we obtained approximate photometry synthesized from the Keck/LRIS spectrum taken 37 days after the first detection. To acquire some estimate for the systematic error involved in synthetic photometry, we compared the scatter of the synthetic photometry acquired from the earlier spectra to the linear interpolation of the light curve in the relevant filter. For the *i*-band filter for which no such data exist, we took the error to be the mean of the uncertainty in the *gr* bands.

We corrected for Galactic extinction using the NASA/IPAC Extragalactic Database[12] (NED), which cites a value of $A_V = 0.121$ mag for this line of sight based on Schlafly & Finkbeiner (2011).

S-corrections (Stritzinger et al. 2002) were estimated for the appropriate filters at the times of the spectra, and by then linearly interpolating the trend for different epochs. This became significant (up to $\sim$0.3 mag) for the P60 *r*-band photometry since at the redshift of SN 2016hil the evolving Hα feature is at the boundary of the filter (see Figure 2). Absolute magnitude light curves are thus plotted separately.

Table 2 reports the measured *gri* magnitudes for the Palomar data, as well as the late-time photometry from Keck in Section 2.4. The *gri* S-corrected light curve is presented in Figure 3. Photometry is made available on WISeREP. Although the S/N is low, we suggest that the light curve of SN 2016hil has a double peak, which can also be corroborated by the lower panel of Figure 3.

2.4. Late-time Observations

On the nights of 2017 June 24 ($t = 246$ days) and 2018 December 1 ($t = 771$ days) we obtained simultaneous *r* and *g*

[10] https://www.sdss3.org/dr10/algorithms/sdssUBVRITransform.php
[11] https://github.com/EranOfek/MAAT
[12] https://ned.ipac.caltech.edu/extinction_calculator

Table 2
Ground-based Optical Photometry of SN 2016hil

Δt (day)[a]	Instrument	Filter	AB Mag	BC (mag)[b]
−10.07	P48	*r*	21.49 ± 0.61	0.055[c]
0.00	P48	*r*	20.30 ± 0.12	
4.00	P200/DBSP[d]	*r*	21.04 ± 0.73	···
9.00	Keck/LRIS[d]	*r*	20.17 ± 0.73	···
11.00	Keck/LRIS[d]	*r*	20.97 ± 0.73	···
12.86	P60/SEDM	*r*	21.78 ± 0.34	···
13.82	P60/SEDM	*r*	21.55 ± 0.26	···
14.99	P48	*r*	21.42 ± 0.31	
31.79	P60/SEDM	*r*	20.95 ± 0.18	···
32.91	P48	*r*	20.43 ± 0.21	···
37.00	Keck/LRIS[d]	*r*	22.25 ± 0.73	···
246.29	Keck/LRIS	*r*	25.32 ± 0.50	···
771.05	Keck/LRIS[e]	*r*	25.96 ± 0.83	···
0.03	P48	*g*	20.24 ± 0.12	0.055
4.00	P200/DBSP[d]	*g*	21.64 ± 0.63	···
9.00	Keck/LRIS[d]	*g*	20.35 ± 0.63	···
11.00	Keck/LRIS[d]	*g*	21.26 ± 0.63	···
11.86	P60/SEDM	*g*	21.17 ± 0.23	0.051
12.87	P60/SEDM	*g*	22.55 ± 0.59	0.051
13.82	P60/SEDM	*g*	21.53 ± 0.24	0.050
25.78	P60/SEDM	*g*	20.75 ± 0.31	0.041
31.79	P60/SEDM	*g*	21.02 ± 0.13	0.035
37.00	Keck/LRIS[d]	*g*	22.33 ± 0.63	0.028
246.29	Keck/LRIS	*g*	26.44 ± 0.46	−0.947
771.05	Keck/LRIS[e]	*g*	27.15 ± 0.73	···
4.00	P200/DBSP[d]	*i*	20.91 ± 0.68	···
9.00	Keck/LRIS[d]	*i*	19.91 ± 0.68	···
11.00	Keck/LRIS[d]	*i*	20.57 ± 0.68	···
12.87	P60/SEDM	*i*	20.95 ± 0.24	···
13.82	P60/SEDM	*i*	21.68 ± 0.57	···
31.79	P60/SEDM	*i*	20.51 ± 0.13	···
37.00	Keck/LRIS[d]	*i*	21.75 ± 0.68	···
246.29	Keck/LRIS	*r*+*g*	24.99 ± 0.41	···

Notes.
[a] Relative to the first detection.
[b] Bolometric correction.
[c] Applied on *g*-band photometry derived from the color fit. See details in Section 3.
[d] Synthetic photometry.
[e] 2σ measurements used for limits in Section 3.4.

photometry of SN 2016hil with Keck/LRIS. The 2017 June data consist of four dithered exposures totaling 1290 s in *g* and 1200 s in *r*. The 2018 December data consist of eight dithered exposures totaling 2598 s in *g* and 2400 s in *r*. These data were processed following standard techniques for CCD reductions using `LPipe`.

In order to eliminate contamination by residual light from the nearby galaxy and from surrounding sources, aperture photometry was performed manually: background and background noise were estimated by establishing an elliptical contour of the host and extending it to reach the location of the event. A series of custom apertures (with a radius of 1.″27) were then constructed along this contour, and the background flux was measured with adjustments for any additional flux gradient. The manual measurements were performed in `SAOImageDS9` (Joye & Mandel 2003). The photometric zero-points were acquired using unsaturated stars in the field and by comparing them to the converted SDSS catalog filters as discussed in Section 2.3. Extinction was treated as discussed in Section 2.3, and no S-corrections were applied. In the first epoch, there were faint and marginally significant detections of the transient in *r* and *g* separately. In order to boost the significance of the detection, *r* and *g* images were summed, after manual cross-astrometry was performed using the `Graphical Astronomy and Image Analysis Tool` (`GAIA`; Draper et al. 2014). This resulted in a >3σ detection in the summed image. In Figure 4 a comparison between both epochs in the synthetic $R+g$ band is made, demonstrating the presence of a transient in the first epoch and its absence in the later epoch.

3. Results

3.1. Light Curves

SN 2016hil has peculiar photometric properties for a spectroscopically regular SN II. These usually present a plateau light curve (IIP) or a linearly declining light curve (IIL). The light curve of SN 2016hil is thus unusual, presenting an apparent double peak in the *gri* bands, as can be corroborated from the lower panel of Figure 3. Although not consistent with a plateau or a linear decline, the photometry is quite noisy. It remains to be seen whether these peculiarities will repeat in similar events in the future. For the rest of the paper, we assume the double peak of the light curve is real. However, none of our main conclusions change if this is not the case.

Unusual for a spectroscopically normal SN II, a double-peaked light curve is more characteristic of Type IIb events (see, e.g., Arcavi 2017 for discussion). The spectroscopic features of SN 2016hil, however, exclude the SN IIb classification, since there are no strong helium signatures and prominent presence of hydrogen persists throughout the spectral evolution. In SNe IIb, double-peaked light curves have been suggested to be the result of a peculiar density structure Bersten et al. (2012). Nakar & Piro (2014) show that such a light curve can be produced by a compact core surrounded by an extended low-mass envelope. In some cases the double-peaked structure is attributed to binary interaction (as shown, for example, by Benvenuto et al. 2013). On the other hand, Sapir & Waxman (2017) claim that such a density structure is not necessary to produce a double peak, which can be produced by a standard progenitor star. In such double-peaked light curves, the first peak is generally thought to be powered by shock cooling, and the second peak is powered by the radioactive decay of ^{56}Ni. The double-peaked light curve of SN 2016hil seems to indicate that the event had a progenitor different than the red supergiant expected for a standard SN II (Smartt 2009 and references therein).

3.2. Bolometric Light Curve

We estimated the bolometric light curve of SN 2016hil to see if it is consistent with a radioactively powered light curve, and acquire limits on the corresponding ^{56}Ni mass. The bolometric correction was estimated from *g* magnitudes and the *g*-*r* color, using a quadratic fit to the color based on a sample of SNe II as described by Lyman et al. (2014). Since the color evolution was observed to be linear over the entire period of observations, but color was not available for all epochs, we fit a linear trend and used this fit to compute the bolometric correction for all times where a measurement in either *g* or *r* was available [including the late-time ($t = 37$ days) synthetic photometry point]. The bolometric correction as calculated appears in Table 2. Using the bolometric luminosity, the integrated

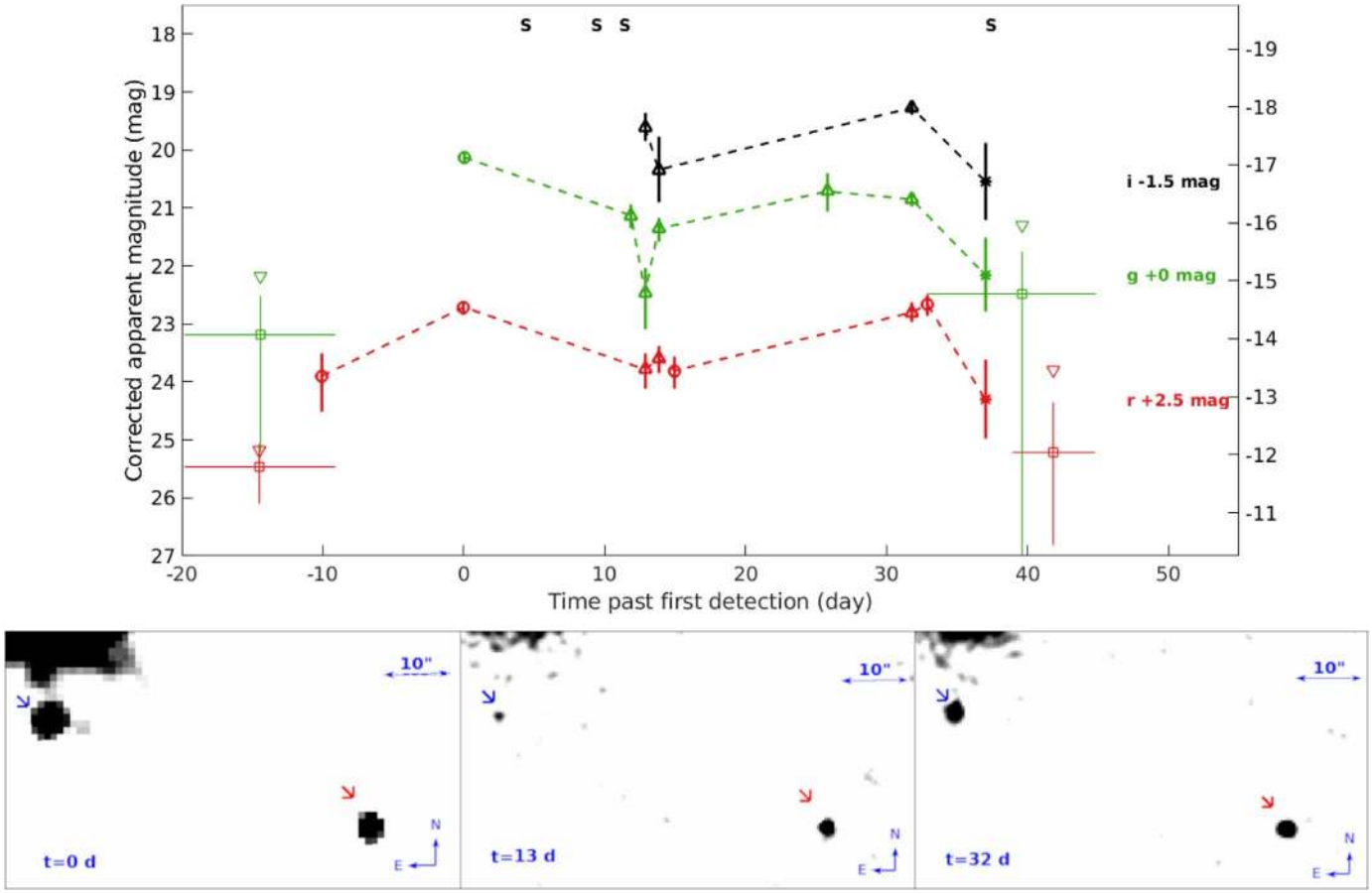

Figure 3. In the top panel are S-corrected optical light curves compiled from P48, P60, and synthetic photometry from the late-time Keck/LRIS spectrum, demonstrating the photometric evolution of SN 2016hil. The data point markers correspond to the instrument used: circles are P48, upward-pointing triangles are P60/SEDM, and stars are synthetic photometry. The square points on the sides of the light curves correspond to summed fluxes (stars) and derived 3σ limits (downward-pointing triangles). The period over which the data were stacked is indicated by the horizontal error bars. Smoothed observations in the r/R bands are presented in the lower panel for reference for $t = 0$, 13, and 32 days. A red arrow points to a nearby source (which is not variable compared to other stars in the field), and a blue arrow points to the location of SN 2016hil. Note the visible decline in brightness at $t = 13$ days, followed by an increase in brightness at $t = 32$ days.

bolometric energy output of the SN is estimated to be $(7.9 \pm 3.5) \times 10^{48}$ erg.

We assume that all late-time luminosity is due to ^{56}Ni decay, and use the following model for ^{56}Ni $\rightarrow^{56}$ Fe decay (see Katz et al. 2013; Nakar et al. 2016; Wygoda et al. 2019). At early times, all γ-rays produced in the decay are scattered and deposit their energy in the ejecta. At late times, only a fraction $f_\gamma \approx t_0^2/t^2$ of the γ-rays deposit their energy in the ejecta, where t_0 is the γ-ray escape time. A common interpolation for the intermediate times is $f_\gamma \approx (1 - e^{-t_0^2/t^2})$, which captures the correct limits at late and early times. Using this, the total energy output produced by ^{56}Ni decay is given by

$$Q_{\rm Ni}(t) = \frac{M_{^{56}\rm Ni}}{M_\odot} f_{\rm dep} \cdot (6.45\, e^{-\frac{t}{8.8\ \rm days}} + 1.44\, e^{-\frac{t}{111.3\ \rm days}}) \times 10^{43}\ \rm erg\ s^{-1},$$

where $f_{\rm dep} = (0.97 f_\gamma + 0.03)$ is the total fraction of deposited energy due to the radioactive decay, including the energy deposited by positrons. Using this expression, we can place a lower bound on the total ^{56}Ni mass at late times by assuming that all the luminosity at 246 days is due to ^{56}Co $\rightarrow^{56}$ Fe decay, and that $f_\gamma = 1$. This gives a lower bound of $M_{^{56}\rm Ni} \geqslant 0.012\, M_\odot$. Alternatively, we can compute the $M_{^{56}\rm Ni}$ for a given t_0.

We can further note that since $\int_0^t Q_{\rm Ni} t' dt' \leqslant \int_0^t L_{\rm bol} t' dt'$ for all times ($\int_0^t L(t') t' dt'$ is a conserved quantity, accounting for adiabatic losses), we can place an upper bound on the ^{56}Ni mass for a given t_0, using the ^{56}Ni mass required to power the entire light curve:

$$\frac{M_{^{56}\rm Ni}}{M_\odot} \leqslant \frac{\int_0^t L_{\rm bol} t' dt'}{\int_0^t f_{\rm dep} \cdot (6.45\, e^{-\frac{t'}{8.8\ \rm days}} + 1.44\, e^{-\frac{t'}{111.3\ \rm days}}) \cdot 10^{43}\ \rm erg\ s^{-1} t' dt'}.$$

Here the late-time observations are assumed to have the minimal value of $f_{\rm dep}$, (corresponding to the maximal amount of ^{56}Ni producing the late-time luminosity), while agreeing with the rest of the light-curve data. This gives an upper limit of $M_{^{56}\rm Ni} \leqslant 0.07\, M_\odot$, above which the ^{56}Ni mass as measured from late times will not agree with the integrated luminosity. We note that this upper limit is somewhat dependent on the starting point of the integration, but will not change our results or conclusions significantly. For example, changing the explosion time to 5 days earlier than the first photometry point

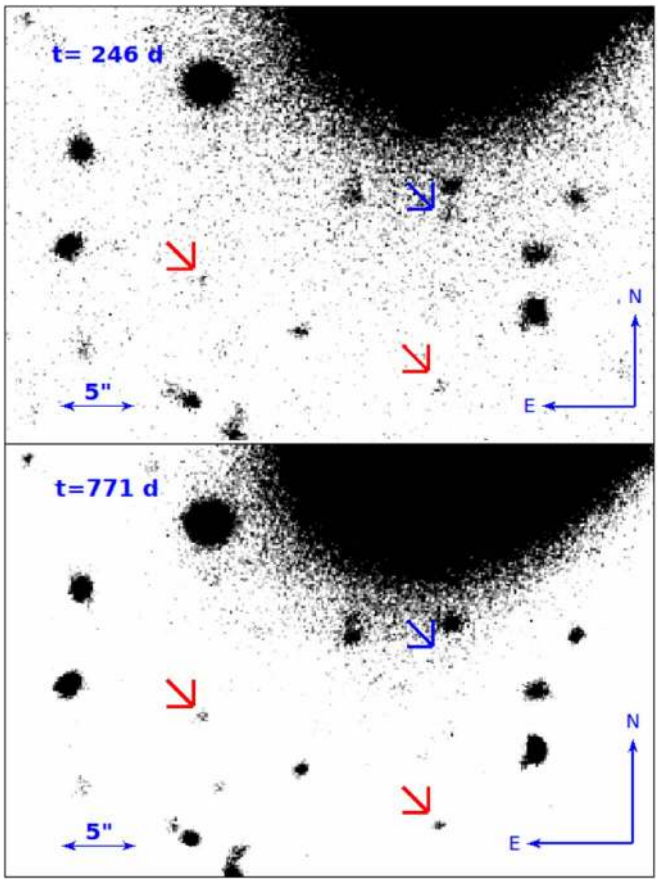

Figure 4. Deep Keck/LRIS $r+g$ observations of the event location at 246 (top panel) and 771 (bottom panel) days after detection (JD 2458454 and JD 2457930, respectively). In both panels, blue arrows point at the location of the event, and red arrows point at sources of comparable brightness for reference. Even though the detection is marginal in the r and g bands separately, it becomes significant when viewed in the $r+g$ summed image.

would increase the upper limit by 30% to $0.09\,M_{\odot}$, which is still well within the typical range for SNe II.

In Figure 5 we present the bolometric luminosity plotted together with the two limiting cases for the energy deposition due to ^{56}Ni decay $M_{^{56}\mathrm{Ni}} = 0.07\,M_{\odot}$, $t_0 = 100$ days and $M_{^{56}\mathrm{Ni}} = 0.012\,M_{\odot}$, $t_0 \to \infty$. We can thus conclude that the late-time photometry of SN 2016hil can provide a ^{56}Ni content consistent with the second peak of the light curve being powered by ^{56}Ni decay.

3.3. Spectral Properties

As can be seen in Figure 2, spectra of SN 2016hil display a strong presence of hydrogen, but few other features were identified. SN 2016hil can thus be classified as a spectroscopically regular SN II. The absorption minima of the P-Cygni profile of the $H\alpha$ feature correspond to expansion velocities of $\sim$5000 km s^{-1} throughout the spectral evolution. Across all spectra, this Hα absorption minimum is weak relative to those of other Blamer features. This is more characteristic of an SN IIL than of an SN IIP (see, e.g., Figure 18 in Arcavi 2017). In all spectra, there are no indications of narrow host emission lines, which could serve as indicators of SF. In the spectrum taken 11 days after detection, an unidentified broad emission feature appears near 6300 Å. It is not seen in the spectrum taken 2 days earlier, probably owing to the low S/N. The lack

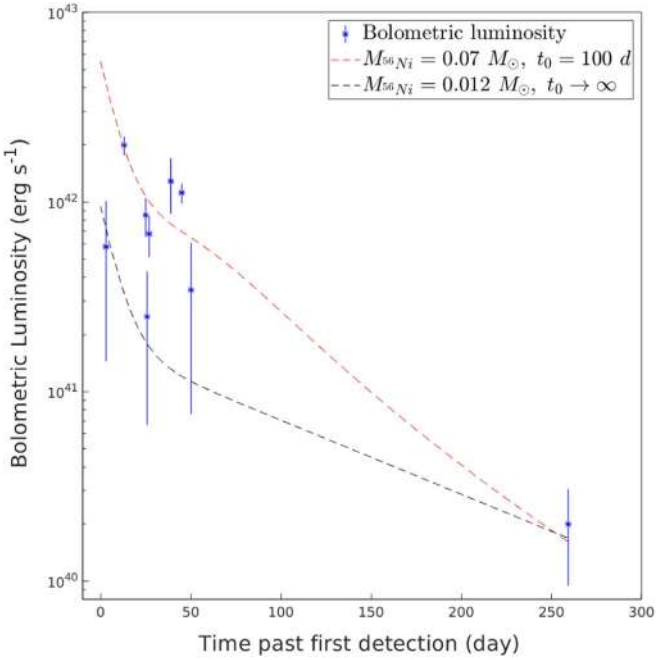

Figure 5. Bolometric luminosity of SN 2016hil (blue points), plotted with ^{56}Ni decay energy deposition rate for two limiting cases: $M_{^{56}\mathrm{Ni}} = 0.07\,M_{\odot}$, $t_0 = 100$ days (red dashed line), and $M_{^{56}\mathrm{Ni}} = 0.012\,M_{\odot}$, $t_0 \to \infty$ (black dashed line).

of other features seems to indicate a low metallicity, which is expected from a low-luminosity host galaxy (i.e., according to the mass-Z relation; Tremonti et al. 2004). However, since a metallicity gradient is present in many galaxies (e.g., Sánchez et al. 2014) the low metallicity of the event could also be consistent with the environment in the outskirts of the main host galaxy.

In a sample by Taddia et al. (2016), the strength of the Fe II λ 5018 feature was used to determine the metallicity according to the method of Dessart et al. (2014). In Figure 6 we put the spectra of SN 2016hil in context with such SNe, including PTF10gxi and PTF12ftc, for which the metallicity was determined to be $Z = 0.4Z_{\odot}$. The fact that the Fe II λ 5018 feature is visible in the spectra of both SNe, and not in any of the spectra of SN 2016hil, suggests that it has a similar or lower metallicity content (e.g., Anderson et al. 2016, 2018).

The continua of the spectra were fitted to blackbody emission. This was done by iteratively fitting a continuum, subtracting it, removing outliers, and refitting the remaining data, until the temperature converges. In all spectra, the temperature was found to be close to 7000 K, without a clear trend in time. Uncertainties were estimated using 68% confidence bounds, not accounting for systematic errors. The fitted temperatures and their corresponding uncertainties appear in Table 3.

3.4. Host Galaxy

Identifying the host of SN 2016hil with certainty is crucial for putting this event in context. Our initial association of SN 2016hil with the galaxy SDSS J011024.51+141238.7 is primarily due to SN 2016hil having a redshift consistent with that of the nearby galaxy. We compared the host spectrum, acquired from the SDSS Science Archive Server (SAS), to

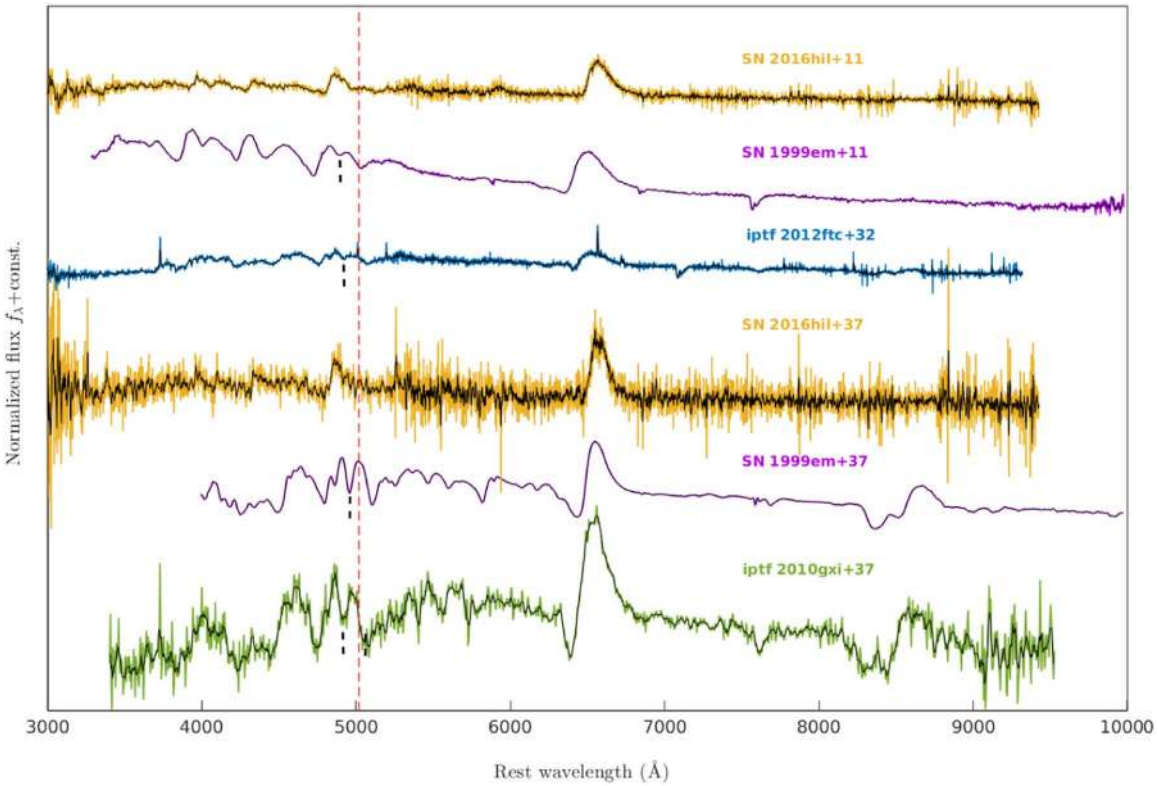

Figure 6. Spectra of SN 2016hil at 11 and 37 days after peak brightness compared with other SNe II at similar phases. Each spectrum is plotted together with a smoothed counterpart (solid black curves). The dashed red line is the Fe II λ 5018 line at rest wavelength. The absorption minimum is marked with a solid black line in spectra where the feature is visible.

Table 3
Blackbody Fits for SN 2016hil

Date	Δt (day)	Temperature (K)
2016 Oct 26	4	6462 ± 40
2016 Oct 31	9	7648 ± 38
2016 Nov 2	11	6709 ± 16
2016 Nov 28	37	7134 ± 46

Note. Relative to first detection.

templates of various galaxy types (Kinney et al. 1996). It is most consistent with being an elliptical galaxy.

To put this host in context of the general population of host galaxies of SNe II, we compare its photometric properties to the host galaxies of the (i)PTF CCSN sample (S. Schulze et al. 2019, in preparation). This homogeneous sample consists of 503 SNe II, detected between the beginning of 2009 and the beginning of 2017. We retrieved archival images of the host galaxy from *Galaxy Evolution Explorer* (*GALEX*) Data Release (DR) 8/9 (Martin et al. 2005), SDSS DR9 (Ahn et al. 2012), PS1 DR1 (Chambers et al. 2016), the Two-Micron All Sky Survey (2MASS; Skrutskie et al. 2006), and the unWISE (Lang 2014) images from the NEOWISE (Meisner et al. 2017) Reactivation Year 3. Furthermore, we use the matched-aperture photometry software package `Lambda Adaptive Multi-Band Deblending Algorithm in R` (`LAMBDAR`; Wright et al. 2016) that is based on a photometry software package developed by Bourne et al. (2012) and tools which will be presented by S. Schulze et al. (2019, in preparation). The photometry was either calibrated against zero-points (*GALEX*, PS1, SDSS, and NeoWISE) or against a set of stars (2MASS). The resulting photometry is summarized in Table 4.

Table 4
Multiwavelength Magnitudes of the Host Galaxy

Instrument/ Filter	$\lambda_{\rm eff}$ (Å)	Magnitude
GALEX/FUV	1542	20.14 ± 0.11
GALEX/NUV	2274	20.77 ± 0.47
SDSS/u	3595	17.85 ± 0.08
SDSS/g	4640	16.03 ± 0.03
SDSS/r	6122	15.13 ± 0.03
SDSS/i	7440	14.65 ± 0.02
SDSS/z	8897	14.26 ± 0.03
PS1/$g_{\rm PS1}$	4776	15.98 ± 0.03
PS1/$r_{\rm PS1}$	6130	15.20 ± 0.01
PS1/$i_{\rm PS1}$	7485	14.72 ± 0.01
PS1/$z_{\rm PS1}$	8658	14.53 ± 0.02
PS1/$y_{\rm PS1}$	9603	14.21 ± 0.02
2MASS/J	12,482	14.18 ± 0.05
2MASS/H	16,620	13.87 ± 0.05
2MASS/K_s	21,590	14.04 ± 0.05
NEOWISE/$W1$	33,526	14.49 ± 0.01
NEOWISE/$W2$	46,028	15.13 ± 0.03

Note. All measurements are reported in the AB system and are not corrected for reddening. For guidance, we report the effective wavelength of each filter.

As for the (i)PTF CCSN host-galaxy sample, we model the spectral energy distribution (SED) of the host with the software

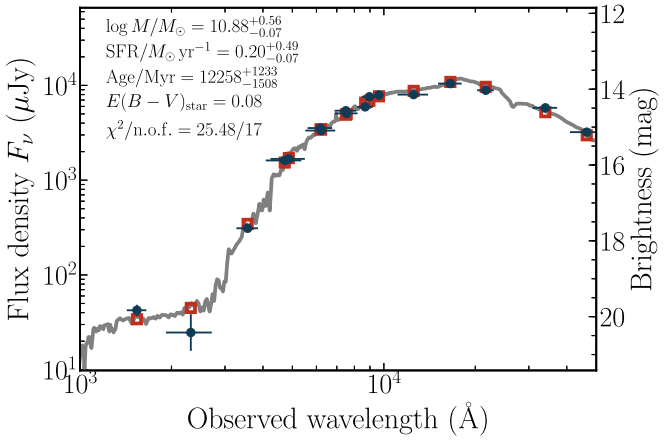

Figure 7. Spectral energy distribution of the elliptical galaxy SDSS J011024.51+141238.7 (blue data points) that could have hosted SN 2016hil. The solid line displays the best fit and the red squares represent the model-predicted photometry. Key properties of the fit are shown in the figure. The quality of the fit is expressed by the χ^2 divided by the number of filters (n.o.f.).

package `LePhare`[13] version 2.2 (Arnouts et al. 1999; Ilbert et al. 2006) and standard assumptions (Bruzual & Charlot 2003 stellar population-synthesis models with the Chabrier initial mass function Chabrier (2003), an exponentially declining star formation history and the Calzetti et al. (2000) attenuation curve).

Figure 7 shows the observed SED. It is best described by a galaxy, dominated by an old stellar population, with a large stellar mass content of $\log(M/M_\odot) = 10.88^{+0.56}_{-0.07}$ and a low SF rate (SFR) of $\mathrm{SFR} = 0.20^{+0.49}_{-0.07}\ M_\odot\ \mathrm{yr}^{-1}$. The age of the stellar population and the large mass corroborate the conclusion from the SDSS spectrum that this is indeed an elliptical galaxy. The low but non-negligible SFR is not in conflict with this interpretation. Schawinski et al. (2007) showed that ∼30% of a volume-limited sample of luminous E galaxies exhibited signs of recent SF. Furthermore, such SF is expected to trace the stellar population of the galaxy, and is not likely to extend to the outskirts.

Another option could be that SN 2016hil occurred in a faint satellite of the main host, where there is still SF activity. As can be seen in Figure 4, the relatively deep Keck/LRIS images reveal no obvious dwarf galaxy or star-forming region at the location of SN 2016hil. Using the low-S/N (2σ) flux detected in the $t = 771$ days epoch in the r and g bands, we attempt to constrain the galaxy mass and SFR of a possible dwarf satellite host. We repeated the SED fitting process using the r and g photometry. The results constrain the presence of a potential dwarf host such that $\log(M/M_\odot) = 7.27^{+0.43}_{-0.24}$, and SFR $\leqslant 0.01\ M_\odot\ \mathrm{yr}^{-1}$. As the SED is based only on g and r photometry, the mass estimate should be regarded as an upper limit. The SFR upper limit is corroborated using a limit derived from the *GALEX*/MIS non-detection in the FUV band, according to the procedure outlined in Kennicutt (1998). Assuming the limiting magnitude of *GALEX*/MIS (∼23.5 mag), we acquire a limit of SFR $\leqslant 0.022\ M_\odot\ \mathrm{yr}^{-1}$, in agreement with the modeling results.

To put both host-galaxy candidates in the context of the general population of SN II host galaxies, we compare their masses and absolute magnitudes to those of the SN II hosts from the (i)PTF survey (Figure 8; values taken from Schulze et al. 2019, in preparation). Both candidate host galaxies have extreme values for an SN II host. The elliptical galaxy is among the most luminous and the most massive galaxies in the sample. At the other extreme, the potential dwarf galaxy cospatial with the SN site would be the least luminous host in the SN II (i)PTF sample with $M_g = -10.1 \pm 0.73$ mag, at least 2 mag fainter than the next faintest host. Combined with the mass limit of $10^{7.3}\ M_\odot$, this puts this object at the very low end of mass and luminosity functions of star-forming galaxies.

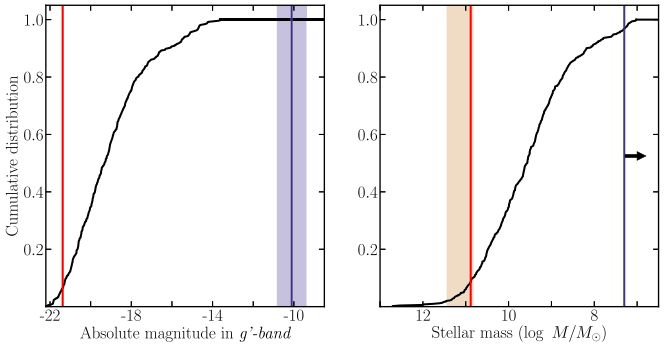

Figure 8. Comparison of the host properties (mass and g-band luminosity) of the two host-galaxy candidates to the general population of SN II host galaxies from the (i)PTF CCSN sample (503 objects; black curves). The properties of the elliptical galaxy SDSS J0110+1412 are shown in red and those of the potential dwarf galaxy are shown in blue. The shaded regions indicate the 1σ uncertainties. Modeling the spectral energy of the dwarf galaxy only provides an upper limit on the stellar mass. This is indicated by the arrow pointing toward lower masses. Uncertainties are not presented in this upper limit.

4. Discussion and Conclusions

Although it is a SN II, SN 2016hil was detected in an unlikely location—the extreme outskirts of an early-type galaxy, where no SF is expected. The SN presented a low-metallicity spectrum with moderate expansion velocities and blackbody temperatures. Its photometry reveals a double-peaked light curve, with late-time photometric observations that are consistent with a ^{56}Ni mass sufficient to power the second peak. This being said, the quality of the photometric data is relatively low. It remains to be seen whether similar future events will exhibit comparable properties.

Deep optical photometry of the environment of SN 2016hil shows no significant sources that could have provided an alternative host where normal SF activity would still be taking place. This, as well as the fact that the nearby galaxy shares the same redshift as SN 2016hil, make it the immediate candidate for being the host of SN 2016hil. Still, we do not have enough data to fully exclude the possibility of a very faint host gravitationally bound to the nearby galaxy. That being said, such a dwarf host would have $M_g > -10.1$ mag and an extremely low stellar content of $<10^{7.3}\ M_\odot$.

Whether such an extreme host exists could be probed with very deep observations in the visible (below our current Keck limits), and any SF can be best probed by deep observations in the UV from *HST*.

SN 2016hil is thus either a peculiar SN in a normal galaxy, or a peculiar SN in a peculiar galaxy. In either case, this unusual host environment could have interesting implications. We outline several possibilities for the origin of SN 2016hil.

(1) The progenitor was formed in the main part of the nearby E host, and was ejected with high velocity. In such a case, the event is tracing a residual population of massive stars

[13] http://www.cfht.hawaii.edu/~arnouts/LEPHARE/lephare.html

in early-type galaxies—the result of the remaining high-mass ($>8\,M_{\odot}$) star formation in the host. Kasliwal et al. (2012) show that the vast majority of SNe occur within 10 kpc of the host-galaxy nucleus. A simple calculation demonstrates that such a star would have to travel with a velocity of $\sim$1000 km s^{-1} in order to travel $\sim$10 kpc within the $\sim$10 Myr of its lifespan. We tentatively conclude that this option does not seem very likely, as it requires two rare phenomena to occur: significant residual SF in an elliptical galaxy and a hypervelocity ejection.

(2) The star was formed locally in a star-forming satellite of the elliptical galaxy, which still produces high-mass stars. This option is favored, as it does not require any modification of the standard paradigm of SN II formation, but is disfavored by the fact that we have strong constraints on the mass and luminosity of a possible host at the location of the event, which can be further tightened in the near future. If this turns out to be the case, SN 2016hil would be the SN II with the faintest host observed by (i)PTF to date. Recently, Sedgwick et al. (2019) demonstrated the existence of a population of low surface brightness galaxies, which host seemingly hostless CCSNe, down to a limit of $10^{6.4}\,M_{\odot}$. This makes this option a possibility that cannot be ignored. Collecting the statistics of such seemingly hostless SNe could provide a handle on the number of almost invisible faint dwarf galaxies in a given volume and redshift.

(3) The progenitor is part of a middle-aged diffuse population of $<8\,M_{\odot}$ stars extending around the host. How can such stars explode as SNe II? Several ideas involving interactions of lower-mass progenitors have been proposed. Zapartas et al. (2017) outline evolutionary channels through which "late" CCSNe (up to 200 Myr after SF) may occur. One option is that a pair of main-sequence (MS) intermediate-mass stars (4–8 $M_{\odot}$), or an intermediate-mass MS star and a post-MS star, could merge completely. Such a merger would revive the merger product, which will recover its equilibrium structure and eventually terminate in a CCSN. Other options include the reverse merger of a compact object and a post-MS star, resulting in a CCSN after an initial common-envelope phase, as discussed by Sabach & Soker (2014). This evolutionary scenario is reminiscent of the formation of blue stragglers (Sandage 1953). These are thought to form as a result of a merger of two lower-mass MS stars, which increases the H-burning time of their merger product relative to the other members of the cluster, thus delaying their turnoff from the MS (e.g., Lombardi et al. 1995, 1996; Sills et al. 1997, 2001).

These binary interaction scenarios could provide a reasonable explanation for a double-peaked light curve—in the aftermath of a merger, we expect a significant increase in the size of the surrounding envelope. Such an expansion could create a low-mass and extended envelope that could could produce two peaks. This is reminiscent of our current understanding of SNe IIb, where the envelope of a star is thought to be mostly stripped owing to binary interaction, thus revealing the helium core during its spectral evolution. In this case, however, a hydrogen envelope could remain around the merged core, so that the spectral evolution would remain dominated by hydrogen.

Finally, we note that SN 2016hil joins a growing list of objects found at large offsets from the nearest galaxy. As a population, Ca-rich SNe Ib preferentially occur at large offsets ($\geqslant$10 kpc) from their host (Lunnan et al. 2017). Other peculiar cases are the Type Ibn PS1-12sk and the Type Ic iPTF14gqr (De et al. 2018), found with projected separations of 28.1 kpc and $\sim$29 kpc from the nearest host, respectively. In both cases, there are strong limits on the luminosity of an underlying host. It has been suggested that iPTF14gqr is the result of an ultra-stripped SN in a compact binary system that underwent a common-envelope phase.

With the increasing number of SNe detected in the era of automated wide-area transient surveys, new populations of transients are being revealed. We expect that events similar to SN 2016hil will be discovered in the near future, and a population could be established. SN 2016hil shows some potentially peculiar spectroscopic and photometric properties, in addition to its unusual location. Once we discover more SN 2016hil-like events, we can identify their observational characteristics. These will presumably allow us to answer the question of their origin.

We thank A. Ho and K. De for assistance with some of the observations. A.G.-Y. is supported by the EU via ERC grant No. 725161, the ISF, the BSF Transformative program, and a Kimmel award. A.V.F.'s supernova group at U.C. Berkeley is supported by the TABASGO Foundation, the Christopher R. Redlich Fund, Gary and Cynthia Bengier, and the Miller Institute for Basic Research in Science. T.d.J. is a Bengier Postdoctoral Fellow. R.L. is supported by a Marie Skłodowska-Curie Individual Fellowship within the Horizon 2020 European Union (EU) Framework Programme for Research and Innovation (H2020-MSCA-IF-2017-794467). This research has made use of the NASA/IPAC Extragalactic Database (NED), which is operated by the Jet Propulsion Laboratory, California Institute of Technology, under contract with the National Aeronautics and Space Administration (NASA). Part of this research was carried out at the Jet Propulsion Laboratory, California Institute of Technology, under a contract with NASA. Some of the data presented herein were obtained at the W.M. Keck Observatory, which is operated as a scientific partnership among the California Institute of Technology, the University of California, and NASA; the Observatory was made possible by the generous financial support of the W.M. Keck Foundation. The authors wish to recognize and acknowledge the very significant cultural role and reverence that the summit of Maunakea has always had within the indigenous Hawaiian community. We are most fortunate to have the opportunity to conduct observations from this mountain. This work is based in part on observations obtained with the 48 inch Samuel Oschin Telescope and the 60 inch Telescope at the Palomar Observatory as part of the intermediate Palomar Transient Factory (iPTF) project, a scientific collaboration among the California Institute of Technology, Los Alamos National Laboratory, the University of Wisconsin, Milwaukee, the Oskar Klein Center, the Weizmann Institute of Science, the TANGO Program of the University System of Taiwan, and the Kavli Institute for the Physics and Mathematics of the Universe. The SED Machine is based upon work supported by the National Science Foundation under grant No. 1106171.

ORCID iDs

Ido Irani https://orcid.org/0000-0002-7996-8780
Steve Schulze https://orcid.org/0000-0001-6797-1889
Avishay Gal-Yam https://orcid.org/0000-0002-3653-5598
Ragnhild Lunnan https://orcid.org/0000-0001-9454-4639
WeiKang Zheng https://orcid.org/0000-0002-2636-6508
Alexei V. Filippenko https://orcid.org/0000-0003-3460-0103
Thomas de Jaeger https://orcid.org/0000-0001-6069-1139
Peter E. Nugent https://orcid.org/0000-0002-3389-0586
Mansi M. Kasliwal https://orcid.org/0000-0002-5619-4938
Christoffer Fremling https://orcid.org/0000-0002-4223-103X
Umaa Rebbapragada https://orcid.org/0000-0002-2560-3495
Frank J. Masci https://orcid.org/0000-0002-8532-9395
Jesper Sollerman https://orcid.org/0000-0003-1546-6615

References

Ahn, C. P., Alexandroff, R., Allende Prieto, C., et al. 2012, ApJS, 203, 21
Anderson, J. P., Dessart, L., Gutiérrez, C. P., et al. 2018, NatAs, 2, 574
Anderson, J. P., Gutiérrez, C. P., Dessart, L., et al. 2016, A&A, 589, A110
Arcavi, I. 2017, in Handbook of Supernovae, ed. A. W. Alsabti & P. Murdin (Berlin: Springer), 239
Arcavi, I., Gal-Yam, A., Kasliwal, M. M., et al. 2010, ApJ, 721, 777
Arnouts, S., Cristiani, S., Moscardini, L., et al. 1999, MNRAS, 310, 540
Bellm, E. C., Kulkarni, S. R., Graham, M. J., et al. 2019, PASP, 131, 018002
Benvenuto, O. G., Bersten, M. C., & Nomoto, K. 2013, ApJ, 762, 74
Bersten, M. C., Benvenuto, O. G., Nomoto, K., et al. 2012, ApJ, 757, 31
Blagorodnova, N., Neill, J. D., Walters, R., et al. 2018, PASP, 130, 035003
Bourne, N., Maddox, S. J., Dunne, L., et al. 2012, MNRAS, 421, 3027
Bruzual, G., & Charlot, S. 2003, MNRAS, 344, 1000
Calzetti, D., Armus, L., Bohlin, R. C., et al. 2000, ApJ, 533, 682
Chabrier, G. 2003, PASP, 115, 763
Chambers, K. C., Magnier, E. A., Metcalfe, N., et al. 2016, arXiv:1612.05560
Crocker, A. F., Bureau, M., Young, L. M., & Combes, F. 2011, MNRAS, 410, 1197
De, K., Kasliwal, M. M., Ofek, E. O., et al. 2018, Sci, 362, 201
Dessart, L., Gutierrez, C. P., Hamuy, M., et al. 2014, MNRAS, 440, 1856
Draper, P. W., Gray, N., Berry, D. S., & Taylor, M. 2014, GAIA: Graphical Astronomy and Image Analysis Tool, Astrophysics Source Code Library, ascl:1403.024
Filippenko, A. V. 1997, ARA&A, 35, 309
Filippenko, A. V., Chornock, R., Swift, B., et al. 2003, IAUC, 8159, 2
Gal-Yam, A. 2017, in Handbook of Supernovae, ed. A. W. Alsabti & P. Murdin (Berlin: Springer), 195
Graham, M. L., Sand, D. J., Bildfell, C. J., et al. 2012, ApJ, 753, 68
Hakobyan, A. A., Adibekyan, V. Z., Aramyan, L. S., et al. 2012, A&A, 544, A81
Hosseinzadeh, G., McCully, C., Zabludoff, A. I., et al. 2019, ApJL, 871, L9
Ilbert, O., Arnouts, S., McCracken, H. J., et al. 2006, A&A, 457, 841
Irani, I. 2019, Transient Name Server Classification Report No. 2019-199
James, P. A., & Anderson, J. P. 2006, A&A, 453, 57
Joye, W. A., & Mandel, E. 2003, in ASP Conf. Ser. 295, Astronomical Data Analysis Software and Systems XII, ed. H. E. Payne, R. I. Jedrzejewski, & R. N. Hook (San Francisco, CA: ASP), 489
Kasliwal, M., & Cao, Y. 2018, Transient Name Server Discovery Report No. 2018-1623
Kasliwal, M. M., Kulkarni, S. R., Gal-Yam, A., et al. 2012, ApJ, 755, 161
Katz, B., Kushnir, D., & Dong, S. 2013, arXiv:1301.6766
Kaviraj, S., Khochfar, S., Schawinski, K., et al. 2008, MNRAS, 388, 67
Kaviraj, S., Peirani, S., Khochfar, S., Silk, J., & Kay, S. 2009, MNRAS, 394, 1713
Kaviraj, S., Schawinski, K., Devriendt, J. E. G., et al. 2007, ApJS, 173, 619
Kawabata, K. S., Maeda, K., Nomoto, K., et al. 2010, Natur, 465, 326
Kennicutt, R. C., Jr. 1998, ARA&A, 36, 189
Kinney, A. L., Calzetti, D., Bohlin, R. C., et al. 1996, ApJ, 467, 38
Kulkarni, S. R. 2013, ATel, 4807, 1
Lang, D. 2014, AJ, 147, 108
Law, N. M., Kulkarni, S. R., Dekany, R. G., et al. 2009, PASP, 121, 1395
Lombardi, J. C., Jr., Rasio, F. A., & Shapiro, S. L. 1995, ApJL, 445, L117
Lombardi, J. C., Jr., Rasio, F. A., & Shapiro, S. L. 1996, ApJ, 468, 797
Lunnan, R., Kasliwal, M. M., Cao, Y., et al. 2017, ApJ, 836, 60
Lyman, J. D., Bersier, D., & James, P. A. 2014, MNRAS, 437, 3848
Martin, D. C., Fanson, J., Schiminovich, D., et al. 2005, ApJL, 619, L1
Meisner, A. M., Lang, D., & Schlegel, D. J. 2017, AJ, 153, 38
Nakar, E., & Piro, A. L. 2014, ApJ, 788, 193
Nakar, E., Poznanski, D., & Katz, B. 2016, ApJ, 823, 127
Ofek, E. O. 2014, MATLAB package for astronomy and astrophysics, Astrophysics Source Code Library, ascl:1407.005
Oke, J. B., Cohen, J. G., Carr, M., et al. 1995, PASP, 107, 375
Oke, J. B., & Gunn, J. E. 1982, PASP, 94, 586
Perets, H. B., Gal-yam, A., Crockett, R. M., et al. 2011, ApJL, 728, L36
Perets, H. B., Gal-Yam, A., Mazzali, P. A., et al. 2010, Natur, 465, 322
Perley, D. A. 2019, PASP, 131, 084503
Planck Collaboration, Ade, P. A. R., Aghanim, N., et al. 2014, A&A, 571, A16
Sabach, E., & Soker, N. 2014, MNRAS, 439, 954
Sánchez, S. F., Rosales-Ortega, F. F., Iglesias-Páramo, J., et al. 2014, A&A, 563, A49
Sandage, A. R. 1953, AJ, 58, 61
Sanders, N. E., Soderberg, A. M., Foley, R. J., et al. 2013, ApJ, 769, 39
Sapir, N., & Waxman, E. 2017, ApJ, 838, 130
Schawinski, K., Kaviraj, S., Khochfar, S., et al. 2007, ApJS, 173, 512
Schlafly, E. F., & Finkbeiner, D. P. 2011, ApJ, 737, 103
Sedgwick, T. M., Baldry, I. K., James, P. A., & Kelvin, L. S. 2019, MNRAS, 484, 5278
Shappee, B., Prieto, J., Stanek, K. Z., et al. 2014, AAS Meeting Abstracts, 223, 236.03
Sills, A., Faber, J. A., Lombardi, J. C., Rasio, F. A., & Warren, A. R. 2001, ApJ, 548, 323
Sills, A., Lombardi, J. C., Jr., Bailyn, C. D., et al. 1997, ApJ, 487, 290
Skrutskie, M. F., Cutri, R. M., Stiening, R., et al. 2006, AJ, 131, 1163
Smartt, S. J. 2009, ARA&A, 47, 63
Soker, N. 2019, SCPMA, 62, 119501
Stritzinger, M., Hamuy, M., Suntzeff, N. B., et al. 2002, AJ, 124, 2100
Suh, H., Yoon, S.-c., Jeong, H., & Yi, S. K. 2011, ApJ, 730, 110
Taddia, F., Moquist, P., Sollerman, J., et al. 2016, A&A, 587, L7
Tonry, J. L., Denneau, L., Heinze, A. N., et al. 2018, PASP, 130, 064505
Tremonti, C. A., Heckman, T. M., Kauffmann, G., et al. 2004, ApJ, 613, 898
Waldman, R., Sauer, D., Livne, E., et al. 2011, ApJ, 738, 21
Wright, A. H., Robotham, A. S. G., Bourne, N., et al. 2016, MNRAS, 460, 765
Wygoda, N., Elbaz, Y., & Katz, B. 2019, MNRAS, 484, 3941
Wyrzykowski, Ł, Hodgkin, S., Blogorodnova, N., Koposov, S., & Burgon, R. 2012, in 2nd Gaia Follow-up Network for Solar System Objects, ed. P. Tanga & W. Thuillot (Paris: IMCCE), 21
Yaron, O., & Gal-Yam, A. 2012, PASP, 124, 668
York, D. G., Adelman, J., Anderson, J. E., Jr., et al. 2000, AJ, 120, 1579
Zapartas, E., de Mink, S. E., Izzard, R. G., et al. 2017, A&A, 601, A29